Structural Engineering and Mechanics, *Vol. 66, No. 5 (2018) 557-568*
DOI: https://doi.org/10.12989/sem.2018.66.5.557

Nonlinear spectral collocation analysis of imperfect functionally graded plates under end-shortening

S. Amir M. Ghannadpour* and Payam Kiani

Aerospace Engineering Department, Faculty of New Technologies and Engineering, Shahid Beheshti University, G.C, Tehran, Iran

(Received January 27, 2018, Revised March 9, 2018, Accepted March 15, 2018)

Abstract. An investigation is made in the present work on the post-buckling and geometrically nonlinear behaviors of moderately thick perfect and imperfect rectangular plates made-up of functionally graded materials. Spectral collocation approach based on Legendre basis functions is developed to analyze the functionally graded plates while they are subjected to end-shortening strain. The material properties in this study are varied through the thickness according to the simple power law distribution. The fundamental equations for moderately thick rectangular plates are derived using first order shear deformation plate theory and taking into account both geometric nonlinearity and initial geometric imperfections. In the current study, the domain of interest is discretized with Legendre-Gauss-Lobatto nodes. The equilibrium equations will be obtained by discretizing the Von-Karman's equilibrium equations and also boundary conditions with finite Legendre basis functions that are substituted into the displacement fields. Due to effect of geometric nonlinearity, the final set of equilibrium equations is nonlinear and therefore the quadratic extrapolation technique is used to solve them. Since the number of equations in this approach will always be more than the number of unknown coefficients, the least squares technique will be used. Finally, the effects of boundary conditions, initial geometric imperfection and material properties are investigated and discussed to demonstrate the validity and capability of proposed method.

Keywords: spectral collocation method; functionally graded plates; geometric nonlinearity; least squares technique; imperfection; quadratic extrapolation technique

1. Introduction

Functionally graded materials (FGMs) are special case of composite materials in which the material properties vary continuously and heterogeneously through the thickness to avoid weak interfaces. By gradually varying the volume fraction of constituent materials, they can be survived in environments with high temperature gradients. Many linear and nonlinear studies, involving vibration, buckling, post-buckling and dynamic analyses, have been reported to date.

The computational methods commonly adopted in the post-buckling and nonlinear analysis of structures include first semi-analytical methods. Sofiyev (2007) studied the vibration and stability of composite cylindrical shells containing a FG layer subjected to various loads. Ghannadpour and Alinia (2006, 2009) have studied a large deflection behavior of square plate made of functionally graded material in which the solution is obtained by minimization of the total potential energy of the plate. Bakora *et al.* (2015) obtained the post-buckling response of thick plates made of functionally graded material (FGM) subjected to in-plane compressive, thermal and thermo-mechanical loads using Galerkin technique. In second category, many research works such as Huang and Atluri (1995) and Kim and Noor (1996) have been done with Finite Element Method (FEM) that is one of the most general techniques for engineering computations since its invention and its role has become very important in many engineering fields. Buckling and post-buckling finite element analyses of composite structures are usually based on the incremental/iterative approaches or the perturbation method. The discretization strategy in FEM is its significant advantage although, there exist some weakness due to its mesh-based interpolation. Thermal buckling analyses of laminated composite and functionally graded curved shell panels and also sandwich composite panel under elevated temperature loads have been investigated numerically using finite elements by Kar *et al.* (2016), Katariya and Panda (2016) and Katariya *et al.* (2017). The post-buckling behavior of composite and functionally graded curved shell panels have been studied by Kar and Panda (2016, 2017), Kar *et al.* (2017) and Panda and Singh (2009, 2010a, 2011) under edge compression and uniform and non-uniform thermal environment. The nonlinear finite element steps have been employed to discretize the shell panel domain in these studies. Thermal post-buckling behavior of laminated composite shell panels embedded with shape memory alloy (SMA) fiber has been analyzed by Panda and Singh (2010b, 2013a, 2013b, 2013c). Panda and Katariya (2015) have studied free vibration and buckling (mechanical and/or thermal) behavior of laminated composite flat and curved panels using finite element method. Buckling and post-buckling responses and progressive failure of square symmetric laminates with rectangular cutouts under uniaxial compression have been investigated by Singh and Kumar (2008) using FEM. The same analysis about square

*Corresponding author, Ph.D.
E-mail: a_ghannadpour@sbu.ac.ir

ISSN: 1225-4568 (Print), 1598-6217 (Online)

laminates with symmetric lay-up and with rectangular cutout under in-plane shear load has also been done by them (Singh and Kumar 2010).

Finite Strip Method (FSM) can be expressed as a kind of FEM in which strip element is used. In terms of computational costs, not only it makes much shorter runtime and smaller amount of core for solution of comparable accuracy, but also it needs very small amount of input data since the small number of mesh lines involved. Recently, Ovesy, Ghannadpour and his co-workers have made several contributions by developing some variants of FSMs to investigate the behavior of composite and functionally graded structures. Two of these methods, namely spline and semi-analytical methods, have been developed for predicting the nonlinear response of rectangular imperfect laminates under end-shortening strain (Ovesy *et al.* 2005). They also used both formulations for predicting the geometrically nonlinear response of channel sections with simply supported ends when subjected to uniform end-shortening in their plane (Ovesy *et al.* 2006). Ovesy and Ghannadpour (2007) have also analyzed the large deflection finite strip response of functionally graded plates subjected to the normal pressure loading. A new strip formulation was introduced by Ghannadpour and Ovesy (2008) to obtain the exact degradation of stiffness of I-section struts after buckling. Same study has been done by them to investigate buckling and initial post-buckling of flat plates (Ovesy and Ghannadpour 2009). Thermal buckling behavior of functionally graded plates has been analyzed by Ghannadpour *et al.* (2012) with uniform and linear temperature variation. This research was done by defining a new strip which was called a functionally graded strip. After that Ovesy *et al.* (2015) extended the application of the FSM to analysis the post-buckling behavior of functionally graded plates subjected to the three types of thermal loadings, i.e. uniform temperature rise, tent-like temperature distribution and nonlinear temperature change across the thickness. Sherafat *et al.* (2013) studied the application of the FSM for the buckling analysis of FGPs subjected to in-plane compression loading based on the higher order plate theory (HOPT). Also, Sherafat *et al.* (2013) have investigated a semi-analytical finite strip method for analyzing the post-buckling behavior of rectangular composite laminated plates of arbitrary lay-up subjected to progressive end-shortening and to normal pressure loading.

In the third category, many researches are in class of mesh-less methods that have attracted high interest in recent years. Mesh-less methods do not require the generation of meshes as in the finite element method. This property allows scientists to remove at least some part of the difficulties existing in FEM, such as mesh distortion and re-meshing. Several mesh-less methods have so far been developed such as Smooth Particle Hydrodynamics (SPH), Diffuse Element Method (DEM), Element-Free Galerkin Method (EFGM), Mesh-Less Local Petrov-Galerkin (MLPG), Reproducing Kernel Particle Methods (RKPM), and finally Point Interpolation Method (PIM) (Liu and Gu 2001, Wang and Liu 2002), by passing the interpolation function through the values of each node within the interested domain. This method is classified as a finite series representation method or alternatively as a pseudo spectral method.

By using the EFG method, Liu and Chen (2001) investigated the vibration response of thin plates with complicated shape. Liew and Chen (2004) employed a mesh-free approach for buckling analysis of Mindlin plates that are subjected to in-plane point loads. Qian and Batra (2004) studied transient thermoelastic deformations of a thick functionally graded plate with edges held at a uniform temperature and either simply supported or clamped using MLPG. Dai *et al.* (2004) used a mesh-free radial point interpolation method for analysis of functionally graded plates. Belinha and Dinis (2007) conducted the non-linear analysis of laminated plates using EFGM. Mesh-free local Petrov-Galerkin method with radial basis function have been investigated by Gilhooley *et al.* (2007) to analyze thick functionally graded materials using higher order shear deformable plate theory. By using kp-Ritz method derived from RKPM, Lee *et al.* (2009) discussed the thermo-elastic response of functionally graded plate and shells. They also investigated the mechanical and thermal buckling responses of functionally graded plates using element-free kp-Ritz method (Zhao *et al.* 2009). Liu and Chua (2007) developed mesh-free point interpolation method to analyze the static deflection, free vibration and buckling analysis of laminated composite plates using third-order shear deformation plate theory. Lee *et al.* (2010) examined the post-buckling behavior of FGM plates under edge compression and temperature field conditions by using the mesh-free kp-Ritz method. Ferreira *et al.* (2013) conducted the static deformations and free vibration analysis of laminated composite and sandwich plates by collocation with radial basis functions, according to a layer-wise formulation. The dynamic behavior of moderately thick functionally graded conical, cylindrical shells, annular plates, parabolic and circular panels and shells of revolution has been studied by Tornabene (2009) and Tornabene *et al.* (2009). The discretization of the system equations by means of the Generalized Differential Quadrature (GDQ) method led to a standard linear eigenvalue problem, where two independent variables are involved without using the Fourier modal expansion methodology. The effect of agglomeration on the natural frequencies of functionally graded carbon nanotube-reinforced laminated composite plates and shells resting on the elastic foundation and the static response of composite plates and shells reinforced by agglomerated nanoparticles made of Carbon Nanotubes (CNTs) have been investigated by Banić and Tornabene and their co-workers (Banić *et al.* 2017, Tornabene *et al.* 2017). A micromechanical model based on the agglomeration of these nanoparticles has been developed by Fantuzzi *et al.* (2017) to analyze free vibration of arbitrarily shaped functionally graded plates. Several parametric studies have been presented to show the influence of the agglomeration on the free vibrations. The strong form of the equations governing a plate has been solved by means of the Generalized Differential Quadrature (GDQ) method. Tornabene *et al.* (2017) studied free vibration problem of sandwich shell structures with variable thickness and made of FGMs. In their research, several Higher-order Shear Deformation Theories (HSDTs) have been employed and FGM structures have been characterized by variable mechanical properties due to the through-the-thickness variation of the volume fraction

distribution of the two constituents and the arbitrary thickness profile. More recently, Ghannadpour and Barekati (2016) and Ghannadpour *et al.* (2017) studied the effects of initial imperfection on post-buckling and nonlinear behavior of laminated plates using the Chebyshev technique and pseudo spectral method, respectively.

In this paper, a high accuracy mesh-less analysis as a pseudo spectral method with Legendre Basis Functions (LBF) is conducted to investigate the nonlinear behavior of moderately thick functionally graded plates subjected to end-shortening strain. The fundamental equations for moderately thick rectangular plates are derived using first order shear deformation plate theory and taking into account both geometric nonlinearity and initial geometric imperfections. Due to sharp fluctuations at the boundaries and the occurrence of Runge's phenomenon in the case of uniform points arrangement, the domain is discretized with Legendre-Gauss-Lobatto nodes. The equilibrium equations will be obtained by discretizing the Von-Karman's equilibrium equations and also boundary conditions with finite Legendre basis functions. The final set of equilibrium equations is nonlinear and therefore the quadratic extrapolation technique is used to solve them. Since the number of equations in this approach will always be more than the number of unknown coefficients, the least squares technique will be used. The proposed method gives better approximation and prevents any artificial discontinuity in the field and does not require the generation of meshes. This type of method is very simple to implement since no integration is required. The excellent accuracy in function fitting and simple imposition of essential and natural boundary conditions are other features of the present method. Finally, the effects of boundary conditions, initial geometric imperfection and material properties are investigated and discussed to demonstrate the validity and capability of proposed method.

2. Equilibrium equations

A typical initially imperfect functionally graded plate is schematically shown in Fig. 1. The plate has a length $2a$, width $2b$, constant thickness h and a maximum imperfection $\overline{w}_i$ at the center. The domain occupied by the plate is denoted by Ω whose boundary is $\partial\Omega$. First order shear deformation plate theory (FSDT) is considered to obtain the equilibrium equations here.

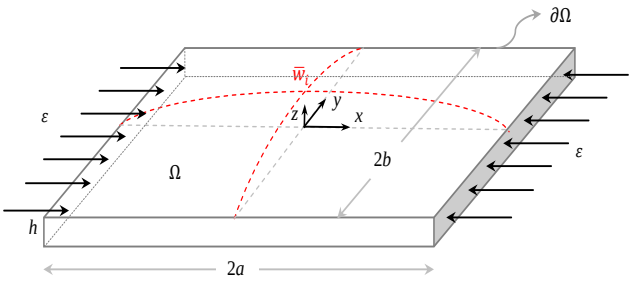

Fig. 1 A typical rectangular FG plate under end-shortening strain

Since the concern here is to investigate the response of a plate to a progressive uniform end-shortening strain, thus the external force does not exist in the current problem. As a result, the total potential energy Π is simply equal to the strain energy U. Therefore, the total potential energy can be obtained by

$$\Pi = \frac{1}{2}\int_V \boldsymbol{\sigma}^T \boldsymbol{e}\, dV = \frac{1}{2}\int_\Omega \int_z \boldsymbol{\sigma}^T \boldsymbol{e}\, dz d\Omega \tag{1}$$

where $\boldsymbol{\sigma}$ is the stresses vector that describes the mechanical state of the problem and can be written as

$$\boldsymbol{\sigma} = \langle \sigma_{xx} \quad \sigma_{yy} \quad \sigma_{xy} \quad \sigma_{xz} \quad \sigma_{yz} \quad \sigma_{zz} \rangle^T = \begin{Bmatrix} \boldsymbol{\sigma}_p \\ \boldsymbol{\sigma}_n \end{Bmatrix} \tag{2}$$

and $\boldsymbol{e}$ is the Green's strains vector as follows

$$\boldsymbol{e} = \langle e_{xx} \quad e_{yy} \quad e_{xy} \quad e_{xz} \quad e_{yz} \quad e_{zz} \rangle^T = \begin{Bmatrix} \boldsymbol{e}_p \\ \boldsymbol{e}_n \end{Bmatrix} \tag{3}$$

As it can be seen, both stresses and strains vectors have been divided to the in-plane and out-of-plane component vectors with subscripts p and n, respectively. These components for strain vectors can be obtained by considering the geometric nonlinearity in the von Karman sense and as the following strain-displacement relations

$$\begin{aligned} \boldsymbol{e}_p &= \mathbb{D}_p \boldsymbol{u} + \frac{1}{2}\left(\mathbb{D}_p \otimes w\right)\mathbb{D}_n \boldsymbol{u} + \left(\mathbb{D}_p \otimes \overline{w}\right)\mathbb{D}_n \boldsymbol{u} \\ &\quad + z\mathbb{D}_p \boldsymbol{\vartheta} = \boldsymbol{\varepsilon}_p + \boldsymbol{\varepsilon}_{nl} + \bar{\boldsymbol{\varepsilon}}_p + z\boldsymbol{\kappa} \\ &= \boldsymbol{\varepsilon}_0 + z\boldsymbol{\kappa} \end{aligned} \tag{4}$$

$$\boldsymbol{e}_n = \mathbb{D}_n \boldsymbol{u} + \boldsymbol{\vartheta} = \boldsymbol{\gamma}$$

where $\otimes$ denotes the Kronecker product and $\boldsymbol{\varepsilon}_0$, $\boldsymbol{\kappa}$ and $\boldsymbol{\gamma}$ are in-plane strains vector, curvatures vector and shear strains vector, respectively. The differential operators $\mathbb{D}_p$ and $\mathbb{D}_n$ are defined as

$$\begin{aligned} \mathbb{D}_p &= \begin{bmatrix} \frac{\partial}{\partial x} & 0 & 0 \\ 0 & \frac{\partial}{\partial y} & 0 \\ \frac{\partial}{\partial y} & \frac{\partial}{\partial x} & 0 \end{bmatrix} = \left[\left(\boldsymbol{\mathcal{D}}_p\right)_{3\times 2} \;\vdots\; (\boldsymbol{0})_{3\times 1} \right] \\ \mathbb{D}_n &= \begin{bmatrix} 0 & 0 & \frac{\partial}{\partial x} \\ 0 & 0 & \frac{\partial}{\partial y} \\ 0 & 0 & 0 \end{bmatrix} = \left[(\boldsymbol{0})_{3\times 2} \;\vdots\; \left(\boldsymbol{\mathcal{D}}_n\right)_{3\times 1} \right] \end{aligned} \tag{5}$$

and $\boldsymbol{u} = \langle u \quad v \quad w \rangle^T$ and $\boldsymbol{\vartheta} = \langle \vartheta_x \quad \vartheta_y \quad 0 \rangle^T$ in which (u, v, w) are the displacement components at the mid-plane, ϑ_x and ϑ_y denote the rotations of the transverse normal about y and x axis, respectively and $\overline{w}$ is initial imperfection of the plate.

With above definitions, the displacements at any point in the functionally graded plate can be obtained by

$$\begin{aligned} d_x(x, y, z) &= u(x, y) + z\vartheta_x \\ d_y(x, y, z) &= v(x, y) + z\vartheta_y \end{aligned} \tag{6}$$

$$d_z(x,y,z) = w(x,y) + \bar{w}(x,y)$$

Nevertheless, all the necessary items in Eq. (1) were introduced except the stress vectors $\boldsymbol{\sigma}_p$ and $\boldsymbol{\sigma}_n$. On the assumption that the plate is in a state of plane stress ($\sigma_{zz} = 0$), the constitutive equations for the FGM plates are

$$\boldsymbol{\sigma}_p = \boldsymbol{Q}_p \boldsymbol{e}_p; \quad \boldsymbol{Q}_p = \begin{bmatrix} Q_{11} & Q_{12} & 0 \\ Q_{12} & Q_{11} & 0 \\ 0 & Q_{26} & Q_{66} \end{bmatrix}$$
$$\boldsymbol{\sigma}_n = \boldsymbol{Q}_n \boldsymbol{e}_n; \quad \boldsymbol{Q}_n = \begin{bmatrix} Q_{44} & 0 & 0 \\ 0 & Q_{55} & 0 \\ 0 & 0 & 0 \end{bmatrix} \tag{7}$$

Where

$$Q_{11} = \frac{E_{(z)}}{1-\upsilon^2}; \quad Q_{12} = \frac{\upsilon E_{(z)}}{1-\upsilon^2};$$
$$Q_{66} = Q_{44} = Q_{55} = G(z) \tag{8}$$

As it can be seen, the material properties E and G have been assumed to be function of z while the Poisson's ratio υ is constant. As it is clear, a functionally graded plate is made from a mixture of ceramics and metals. The composition is assumed to change in such a way that the upper surface is fully ceramic (shown by surface c at $z = h/2$), whereas the lower surface is completely metal (designated by surface m at $z = -h/2$). So, it is considered that the material properties of FGM plate such as the modulus of elasticity E and shear modulus G vary in the thickness direction z by a function $\varrho(z)$ which is defined here by simple power law distribution as

$$\varrho(z) = \varrho_{cm}\left(\frac{2z+h}{2h}\right)^n + \varrho_m \tag{9}$$

It is re-emphasized that the Poisson's ratio υ is assumed to be constant. In Eq. (9), ϱ_m and ϱ_c denote values of the variables at surface m and surface c of the plate, respectively and $\varrho_{cm} = \varrho_c - \varrho_m$.

Using Eqs. (1)-(9) to form the total potential energy and integrating through the thickness with respect to z gives an expression for Π which can be shown as

$$\Pi = \frac{1}{2}\int_\Omega \langle \boldsymbol{\varepsilon}_0^T \quad \boldsymbol{\kappa}^T \quad \boldsymbol{\gamma}^T \rangle \begin{bmatrix} \boldsymbol{E_{1p}} & \boldsymbol{E_2} & 0 \\ \boldsymbol{E_2} & \boldsymbol{E_3} & 0 \\ 0 & 0 & \boldsymbol{E_{1n}} \end{bmatrix} \begin{Bmatrix} \boldsymbol{\varepsilon}_0 \\ \boldsymbol{\kappa} \\ \boldsymbol{\gamma} \end{Bmatrix} d\Omega \tag{10}$$

Where $\boldsymbol{E}_{1p}$ is named extensional stiffness matrix, $\boldsymbol{E}_3$ the bending stiffness matrix, $\boldsymbol{E_2}$ the bending-extensional coupling stiffness matrix and $\boldsymbol{E_{1n}}$ is shear stiffness matrix which are given by

$$\begin{Bmatrix} \boldsymbol{E_{1p}} \\ \boldsymbol{E_2} \\ \boldsymbol{E_3} \\ \boldsymbol{E_{1n}} \end{Bmatrix} = \int_{-h/2}^{h/2} \begin{Bmatrix} \boldsymbol{Q}_p \\ z\boldsymbol{Q}_p \\ z^2\boldsymbol{Q}_p \\ K\boldsymbol{Q}_n \end{Bmatrix} dz \tag{11}$$

Where K is the shear correction factor. The plate internal actions, namely, the membrane stress resultants per unit length $\boldsymbol{N} = \langle N_{xx} \quad N_{yy} \quad N_{xy} \rangle^T$, the transverse stress resultants per unit length $\boldsymbol{Q} = \langle Q_{xx} \quad Q_{yy} \quad 0 \rangle^T$, and the moments per unit length $\boldsymbol{M} = \langle M_{xx} \quad M_{yy} \quad M_{xy} \rangle^T$ are obtained by integrating the stresses through the uniform thickness and they are expressed as

$$\begin{Bmatrix} \boldsymbol{N} \\ \boldsymbol{M} \\ \boldsymbol{Q} \end{Bmatrix} = \int_{-h/2}^{h/2} \begin{Bmatrix} \boldsymbol{\sigma}_p \\ z\boldsymbol{\sigma}_p \\ \boldsymbol{\sigma}_n \end{Bmatrix} dz \tag{12}$$

Therefore

$$\begin{Bmatrix} \boldsymbol{N} \\ \boldsymbol{M} \\ \boldsymbol{Q} \end{Bmatrix} = \begin{bmatrix} \boldsymbol{E_{1p}} & \boldsymbol{E_2} & 0 \\ \boldsymbol{E_2} & \boldsymbol{E_3} & 0 \\ 0 & 0 & \boldsymbol{E_{1n}} \end{bmatrix} \begin{Bmatrix} \boldsymbol{\varepsilon_0} \\ \boldsymbol{\kappa} \\ \boldsymbol{\gamma} \end{Bmatrix} \tag{13}$$

The nonlinear governing equations of equilibrium can be obtained from the total potential energy Π by performing the well-established calculus of variations procedure. Therefore, by employing the Euler-Lagrange equations, the nonlinear equilibrium equations based on FSDT can be compactly written as

$$\begin{bmatrix} \boldsymbol{\mathcal{D}}_p^T & \boldsymbol{0} & \boldsymbol{0} \\ \boldsymbol{\mathcal{D}}_n^T(\mathbb{D}_p^T \otimes d_z) & \boldsymbol{0} & \boldsymbol{\mathcal{D}}_n^T \\ \boldsymbol{0} & \boldsymbol{\mathcal{D}}_p^T & -\boldsymbol{I} \end{bmatrix} \begin{Bmatrix} \boldsymbol{N} \\ \boldsymbol{M} \\ \boldsymbol{Q} \end{Bmatrix} = \{\boldsymbol{0}\} \tag{14}$$

where $\boldsymbol{I}$ is defined here as

$$\boldsymbol{I} = \begin{bmatrix} 1 & 0 & 0 \\ 0 & 1 & 0 \end{bmatrix} \tag{15}$$

3. Solution methodology

In order to solve the equilibrium equations based on FSDT, they should be expressed in terms of the displacements by substituting the force and moment resultants from Eq. (13) into Eq. (14).

As mentioned before, to solve the above equations in this paper, pseudo spectral method or spectral collocation method is selected. Series expansions in orthogonal polynomials are useful to solve many types of boundary value problems. To use a truncated series as an approximation, it is important that the series coefficients decay rapidly. One of the most important polynomials to find the solution of PDEs is the Legendre polynomials $L_k(x)$. Legendre polynomials satisfy the three-term recursion as Eq. (16)

$$L_{k+1}(x) = \frac{2k+1}{k+1} x L_k(x) - \frac{k}{k+1} L_{k-1}(x) \tag{16}$$

Where $L_0(x) = 1$ and $L_1(x) = x$. The derivatives of these polynomials can be obtained by the following relationship

$$(2k+1)L_k(x) = L'_{k+1}(x) - L'_{k-1}(x) \tag{17}$$

Therefore, by selecting the Legendre polynomials as basis functions, the displacement fields in the context of FSDT are approximated by the following relations

$$u = \sum_{i=1}^{N_t}\sum_{j=1}^{N_t} \alpha_{ij}^u L_{i-1}\left(\frac{x}{a}\right) L_{j-1}\left(\frac{y}{b}\right) \tag{18}$$

$$v=\sum_{i=1}^{N_t}\sum_{j=1}^{N_t}\alpha_{ij}^{v}\,L_{i-1}\left(\frac{x}{a}\right)L_{j-1}\left(\frac{y}{b}\right)$$

$$w=\sum_{i=1}^{N_t}\sum_{j=1}^{N_t}\alpha_{ij}^{w}\,L_{i-1}\left(\frac{x}{a}\right)L_{j-1}\left(\frac{y}{b}\right)$$

$$\vartheta_x=\sum_{i=1}^{N_t}\sum_{j=1}^{N_t}\alpha_{ij}^{\vartheta_x}\,L_{i-1}\left(\frac{x}{a}\right)L_{j-1}\left(\frac{y}{b}\right)$$

$$\vartheta_y=\sum_{i=1}^{N_t}\sum_{j=1}^{N_t}\alpha_{ij}^{\vartheta_y}\,L_{i-1}\left(\frac{x}{a}\right)L_{j-1}\left(\frac{y}{b}\right)$$

Where $\alpha_{ij}^{u},\alpha_{ij}^{v},\alpha_{ij}^{w},\alpha_{ij}^{\vartheta_x}$ and $\alpha_{ij}^{\vartheta_y}$ are the unknown coefficients that should be found and N_t is the number of terms in the series expansion.

By substituting the above displacement fields into Eq. (14), nonlinear equations can be obtained in terms of unknown parameters in the space domain Ω. To solve these expanded nonlinear equations, one may consider N_D nodes inside the domain Ω $(\mathbf{x}_\xi \in \Omega, \xi = 1,\dots,N_D)$ and N_B nodes on the boundary $\partial\Omega$ $(\mathbf{x}_\xi \in \partial\Omega, \xi = N_D+1,\dots,N)$, with a total number of nodes $N = N_D + N_B$. It should be noticed that in numerical analyses based on use of points interpolation techniques, Runge's phenomenon may occur in which the problem of oscillation at the edges of the domain happens with polynomials of high degree over a set of equi-spaced interpolation points. Therefore, the Legendre-Gauss-Lobatto points should be used in the domain instead of uniform points. Fig. 2 represents a typical scattered set of Legendre-Gauss-Lobatto points $(n \times m = 8 \times 8)$ in a domain Ω. Parameters n and m denote the number of nodes along the x and y directions respectively.

In order to discretize and solve the nonlinear equilibrium equations, the interior nodes $(1{:}N_D)$ are substituted in the equilibrium equations and for points on the boundary $(N_D+1{:}N)$, essential and natural boundary conditions of the problem will be imposed.

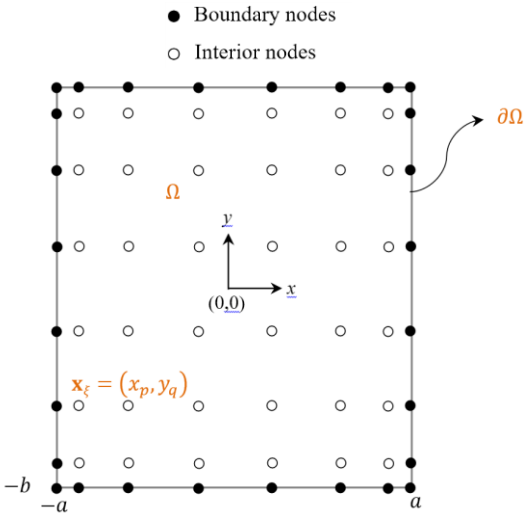

Fig. 2 Legendre-Gauss-Lobatto points in a typical domain Ω

Therefore, all nonlinear equilibrium equations and also all essential and natural boundary conditions of the problem are discretized and obtained in terms of unknown parameters only. Finally, the discretized system of equations for both equilibrium and boundary conditions equations can be expressed as

$$\mathbb{L}\boldsymbol{u}(\mathbf{x}_\xi) = f; \qquad \xi = 1,\dots,N_D \text{ in } \Omega \tag{19}$$

$$\mathbb{L}_B\boldsymbol{u}(\mathbf{x}_\xi) = g; \qquad \xi = \underbrace{N_D+1,\dots,N}_{N_B} \text{ on } \partial\Omega \tag{20}$$

Where $\mathbb{L}$ and $\mathbb{L}_B$ are differential operators in the domain Ω and on the boundary $\partial\Omega$, respectively, f and g are the right-hand side vectors of equations, $\boldsymbol{u}$ is a field variable and $\mathbf{x}_\xi \in (\Omega \cup \partial\Omega), \xi = 1,\dots,N_D$ are Legendre-Gauss-Lobatto points that their coordinates $(x_p, y_q)\big|_{q=1,\dots,m}^{p=1,\dots,n}$ can be used by solving the following equations

$$\begin{cases}\left[1-\left(\frac{x_p}{a}\right)^2\right]\frac{d}{dx}L_p\left(\frac{x_p}{a}\right)=0; & p=1,\dots,n\\ \left[1-\left(\frac{y_q}{b}\right)^2\right]\frac{d}{dy}L_q\left(\frac{y_q}{b}\right)=0; & q=1,\dots,m\end{cases} \tag{21}$$

Nonlinear set of Eqs. (19)-(20) is solved by the well-known and efficient quadratic extrapolation technique in this study. However, in solving the linearized system of equations obtained by quadratic extrapolation technique, it can be observed that the total number of equations is more than the required unknown coefficients. To obtain a unique solution, the well-known least squares technique is also used. In the present study, in order to obtain the converged and accurate results, the convergence criteria should be defined based on both the vector containing the unknown coefficients ($\boldsymbol{d}$) and all equations containing these coefficients i.e., $\mathbf{F}(\boldsymbol{d}) = \langle \mathbb{L}\boldsymbol{u} - f \quad \mathbb{L}_B\boldsymbol{u} - g\rangle^T$. The iterative procedure is repeated until the following conditions be satisfied.

$$\frac{\|\Delta\boldsymbol{d}_r\|}{\|\boldsymbol{d}_{r+1}\|} < 5\times10^{-4} \tag{22}$$

$$\|\mathbf{F}(\boldsymbol{d}_r)\| < 5\times10^{-4} \tag{23}$$

where r is the iteration counter in quadratic extrapolation technique. Once the set of equilibrium equations are solved, the unknown coefficients vector $\boldsymbol{d}$ is found for a prescribed end-shortening strain and therefore, the displacements at any point of the plate can be calculated by using Eq. (18) and both forces and moments can be obtained through use of Eq. (13). In particular, the average longitudinal force N_{av} can be determined by considering the membrane stress resultant N_{xx} and integrating over the domain Ω (using Fig. 3) to give the longitudinal force acting on a plate.

$$N_{av} = \frac{1}{2a}\int_\Omega N_{xx}d\Omega \cong \frac{1}{2a}\sum_{\xi=1}^{N} N_{xx}^{\xi}\Delta A_\xi$$
$$= \frac{1}{8a}\sum_{p=1}^{n}\sum_{q=1}^{m}(x_{p+1}-x_{p-1})(y_{q+1}-y_{q-1})N_{xx}\big|_{y=y_q}^{x=x_p} \tag{24}$$

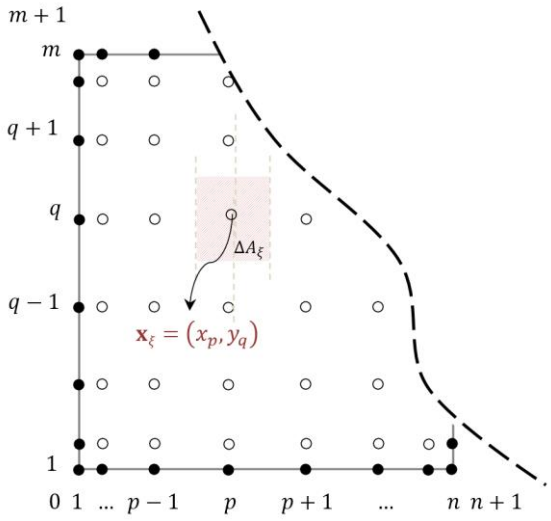

Fig. 3 The bounded area around a node

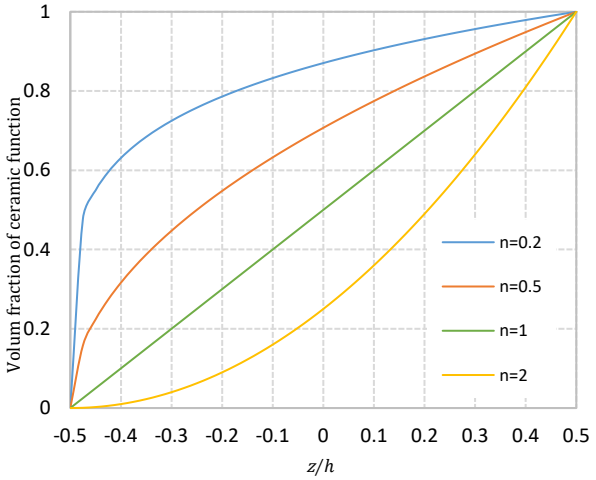

Fig. 4 Variations of volume fraction of ceramic through the thickness

where the parameters x_0, x_{n+1}, y_0 and y_{m+1} have the values correspond to x_1, x_n, y_1 and y_m, respectively.

4. Results and discussions

In this section, in order to show the capability and performance of the proposed formulation, nonlinear and post-buckling analyzes of some moderately thick perfect and geometrically imperfect functionally graded plates are extensively investigated and discussed. Some results obtained by the proposed method will be compared with those extracted form finite element method using ABAQUS commercial software.

4.1 Perfect square FG plates

The analysis of functionally graded plates is conducted for the type of ceramic and metal combination. FGM perfect square plates are studied first to show the capability

Table 1 Material properties of ceramic and metal

Materials	Young's modulus (GPa)	Poisson's ratio
Aluminum	70	0.3
Zirconia	151	0.3

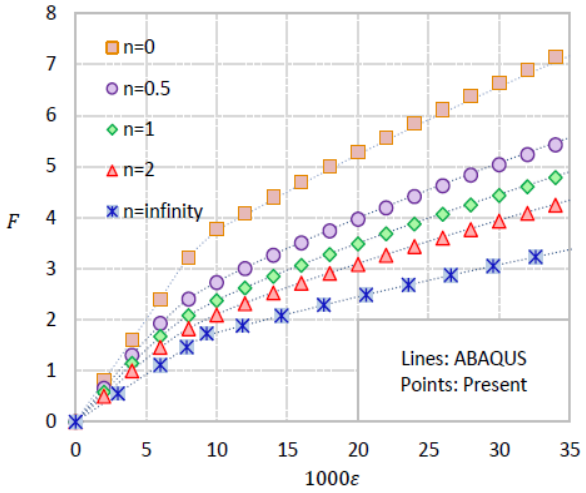

Fig. 5 Variations of longitudinal force versus end-shortening behavior for simply-supported plates

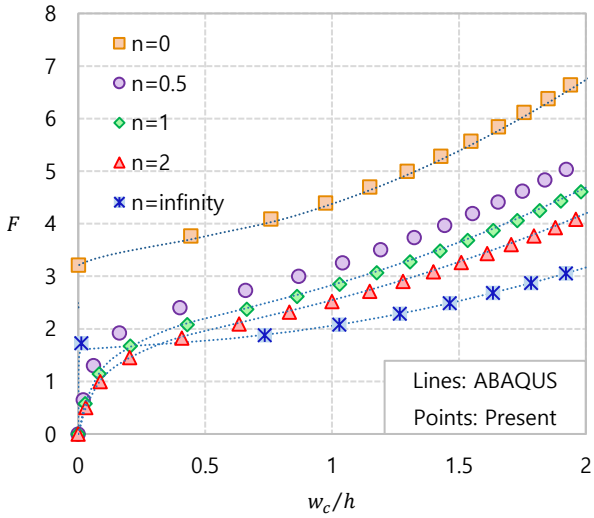

Fig. 6 Longitudinal force-central deflection behavior for simply-supported plates

of the proposed formulation. As noted before, the plates are subjected to uniform end-shortening strain in longitudinal direction and different out-of-plane boundary conditions are also considered. The in-plane boundary conditions are considered in such a way that the loaded ends have lateral expansion and the unloaded edges can move freely.

The materials taken here are zirconia and aluminum. The values of Poisson's ratio for both materials are considered to be constant in this study and the length to thickness ratio $(2a/h)$ is here assumed to be 20. A load factor $F = (2a/E_c h^3)N_{av}$is introduced in presenting the results in which E_c is the elastic modulus of ceramic. It is noted that the results of this study have been obtained by a

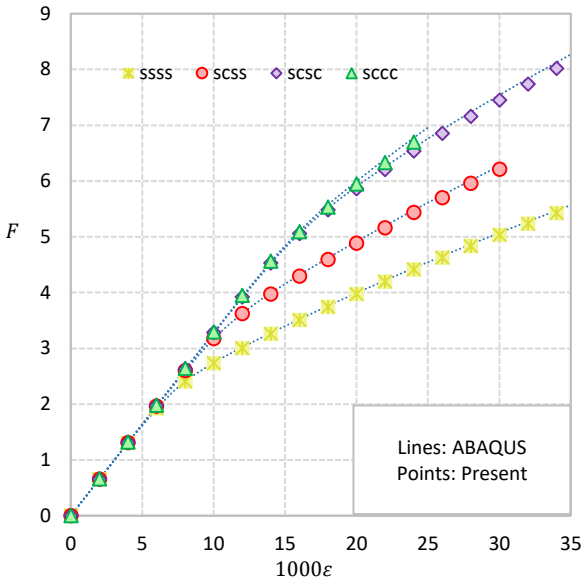

Fig. 7 Variations of longitudinal force versus end-shortening for FGPs with $n = 0.5$ and with different boundary conditions

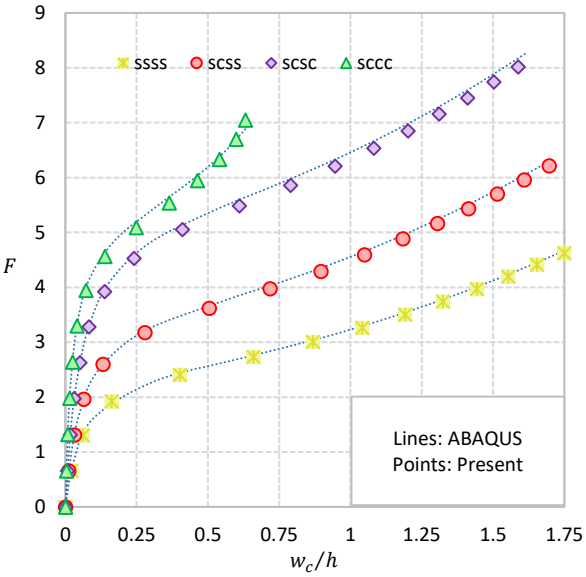

Fig. 8 Longitudinal force-central deflection behavior for FGPs with $n = 0.5$ and with different boundary conditions

thickness of 1 mm.

Table 1 explains the material properties of metal and ceramic and Fig. 4 illustrates the different volume fractions of the ceramic phase through the dimensionless thickness Z $(= z/h)$. In all cases, the upper surface of the plate is assumed to be pure ceramic and the lower is metal.

Figs. 5-6 are illustrated as the load factor-end shortening strain and load factor-maximum deflection history, respectively. The out-of-plane boundary conditions for plates under consideration in this section are simply supported on all edges. All the results presented here have been obtained by taking 11 Legendre basis functions in each

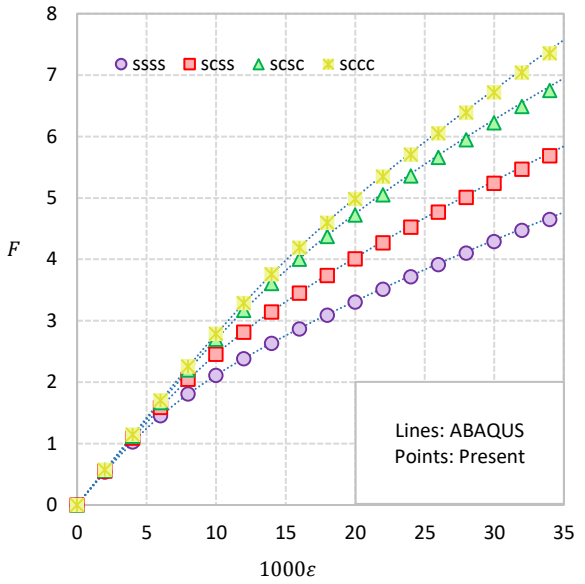

Fig. 9 Variation of longitudinal force versus end-shortening for imperfect FGPs with $n = 1$ and $\bar{w}_i = -0.2h$

direction and for each displacement fields ($N_t = 11$) and by 11×11 nodes located in the domain. The results are compared with those obtained by ABAQUS software. USDFLD subroutine is used to model FGM in ABAQUS and the FGPs are modeled by S4R shell element with total number of 400. As it can be observed, the present results have an excellent agreement with each other.

To demonstrate the ability of the proposed method in modeling different boundary conditions, FG plates with different out-of-plane boundary conditions are investigated here. To do this, four square FGM plates with volume fraction index $n = 0.5$ and for different boundary conditions along both unloaded and loaded edges are analyzed. The in-plane boundary conditions are assumed to be similar to the plates in section 4.1. The results are represented in terms of dimensionless displacements and longitudinal load in Figs.7-8. As it can be seen, the labelling schemes have been included in these figures to assign the related boundary conditions. In these schemes, the first letter refers to the boundary condition applied to the end $x = -a$ and the second letter specifies the relevant boundary condition on the unloaded edge $y = -b$. The sequence will continue in a counter-clockwise direction around the plates. It may be observed from these figures that the plates with more clamped boundary conditions on edges are much stiffer than plate having more simply supported conditions. Therefore, as it can be observed from Fig. 8, the plate with more clamped boundaries has lower out-of-plane deflection at the same level of loading.

4.2 Functionally graded plates with symmetric imperfection

Here an FGM plate with initial imperfection in the form of a single half cosine-wave is analyzed. The plate is assumed to be moderately thick with $2a/h = 20$ and

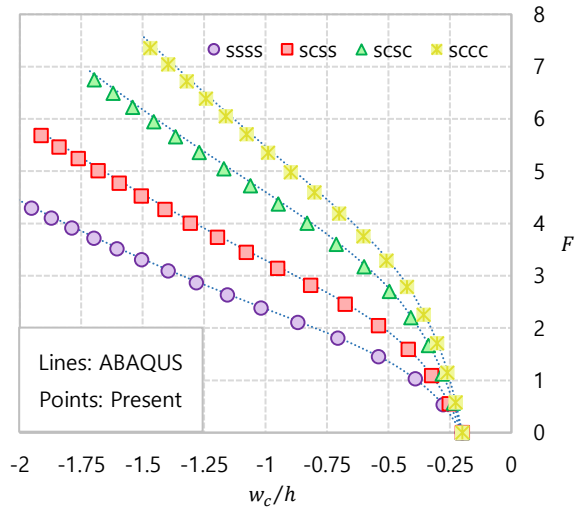

Fig. 10 Longitudinal force-central deflection behavior for imperfect FGPs with $n = 1$ and $\bar{w}_i = -0.2h$

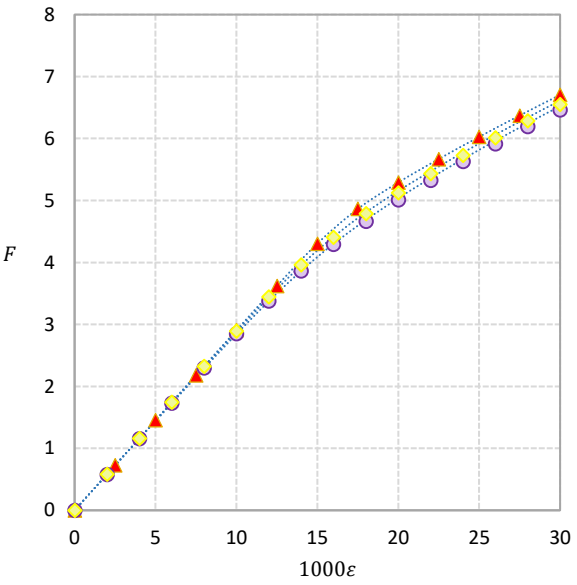

Fig. 11 Variation of longitudinal force versus end-shortening for imperfect FGPs with $n = 1$ with positive and negative imperfections

therefore FSDT formulations should be used to obtain accurate results and the material properties are assumed to be similar to section 4.1. Free in-plane lateral expansion is assumed at both loaded and unloaded edges. Different out-of-plane boundary conditions are reconsidered here. Mathematical models for above mentioned FG plates with different boundary conditions can be expressed as:

For SSSS FG plate

$$\begin{aligned} &u = +\varepsilon a; w = \vartheta_y = 0; N_{xy} = M_{xx} = 0 \; at \;\; x = -a \\ &w = \vartheta_x = 0; \; N_{xy} = N_{yy} = M_{yy} = 0 \quad at \;\; y = -b \\ &u = -\varepsilon a; w = \vartheta_y = 0; N_{xy} = M_{xx} = 0 \; at \;\; x = +a \\ &w = \vartheta_x = 0; \; N_{xy} = N_{yy} = M_{yy} = 0 \quad at \;\; y = +b \end{aligned} \tag{25}$$

For SCSS FG plate

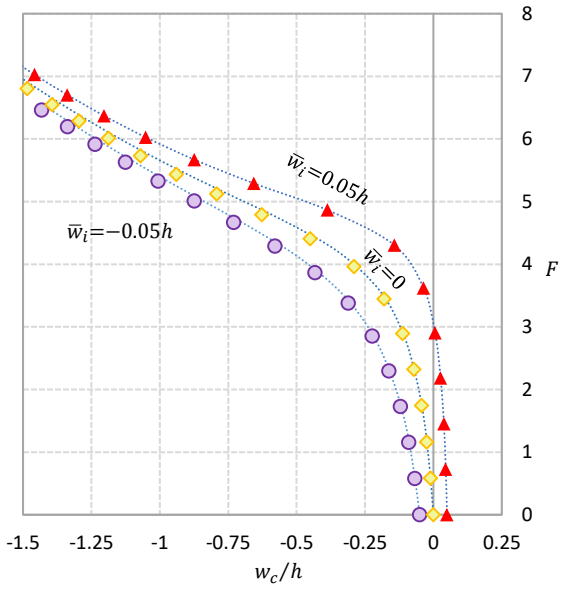

Fig. 12 Longitudinal force-central deflection behavior for imperfect FGPs with $n = 1$ with positive and negative imperfections

$$\begin{aligned} &u = +\varepsilon a; w = \vartheta_y = 0; N_{xy} = M_{xx} = 0 \; at \;\; x = -a \\ &w = \vartheta_y = \vartheta_x = 0; \; N_{xy} = N_{yy} = 0 \quad at \;\; y = -b \\ &u = -\varepsilon a; w = \vartheta_y = 0; N_{xy} = M_{xx} = 0 \; at \;\; x = +a \\ &w = \vartheta_x = 0; \; N_{xy} = N_{yy} = M_{yy} = 0 \quad at \;\; y = +b \end{aligned} \tag{26}$$

For SCSC FG plate

$$\begin{aligned} &u = +\varepsilon a; w = \vartheta_y = 0; N_{xy} = M_{xx} = 0 \; at \;\; x = -a \\ &w = \vartheta_y = \vartheta_x = 0; \; N_{xy} = N_{yy} = 0 \quad at \;\; y = -b \\ &u = -\varepsilon a; w = \vartheta_y = 0; N_{xy} = M_{xx} = 0 \; at \;\; x = +a \\ &w = \vartheta_y = \vartheta_x = 0; \; N_{xy} = N_{yy} = 0 \quad at \;\; y = +b \end{aligned} \tag{27}$$

and for SCCC FG plate

$$\begin{aligned} &u = +\varepsilon a; w = \vartheta_y = 0; N_{xy} = M_{xx} = 0 \; at \;\; x = -a \\ &w = \vartheta_y = \vartheta_x = 0; \; N_{xy} = N_{yy} = 0 \quad at \;\; y = -b \\ &u = -\varepsilon a; w = \vartheta_y = \vartheta_x = 0; N_{xy} = 0 \quad at \;\; x = +a \\ &w = \vartheta_y = \vartheta_x = 0; \; N_{xy} = N_{yy} = 0 \quad at \;\; y = +b \end{aligned} \tag{28}$$

A load factor, similar to section 4.1, is assumed here to present the results. Four square FGM plates with linear variation of plates ingredients ($n = 1$) and with different boundary conditions along the loaded and unloaded edges which include maximum initial imperfection of $\bar{w}_i = -0.2h$ at center of the plates are assumed and analyzed in this section. The results are represented in terms of dimensionless displacements and longitudinal load in Figs. 9-10. The same labelling schemes are also used in these figures to assign the related boundary conditions.

Conclusions similar to those previously made for plates containing clamped boundary conditions are also seen in these figures. The results presented here are also compared with those obtained by finite element method. The FEM analyzes have been carried out using general purpose ABAQUS software. The three-dimensional shell element (S4R) of the ABAQUS library has been used and USDFLD

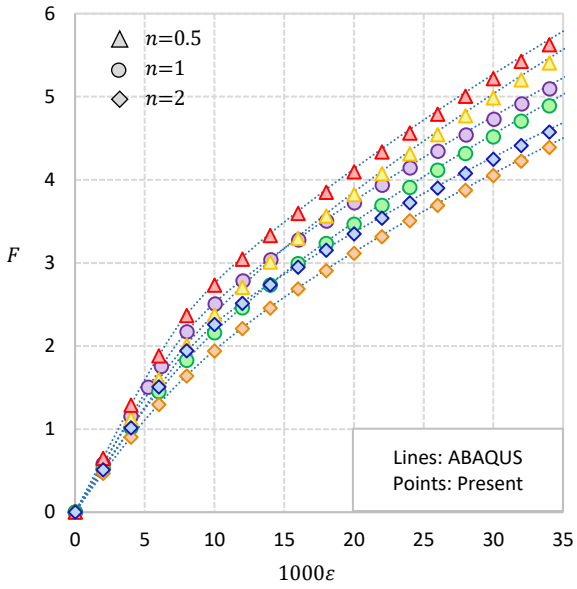

Fig. 13 Variation of longitudinal force versus end-shortening for FGPs with un-symmetric imperfections $\bar{w}_c = 0.2h$ and $\bar{w}_c = 0.5h$

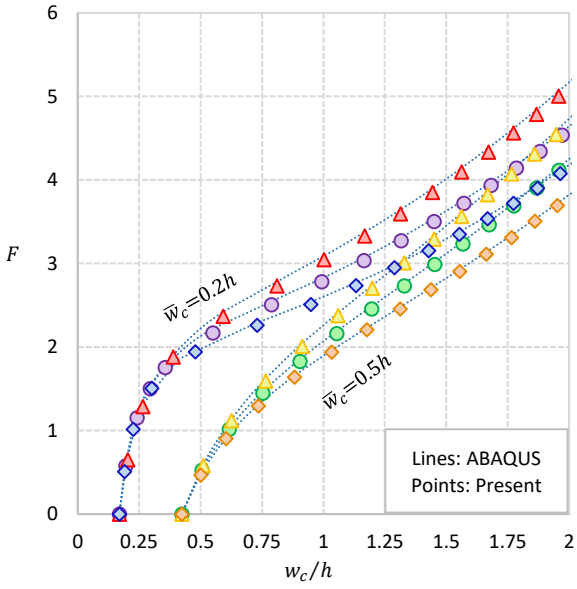

Fig. 14 Longitudinal force-central deflection for FGPs with un-symmetric imperfections $\bar{w}_c = 0.2h$ and $\bar{w}_c = 0.5h$

subroutine code is used again to model FGM. A mesh arrangement composed of 400 square elements with uniform size is used to obtain the accurate results.

Same study has been done for imperfect functionally graded plates with maximum initial imperfections $\bar{w}_i = \pm 0.05h$. It is emphasized that both positive and negative symmetric imperfections are considered here to show the contrast between the bending-extensional coupling stiffness matrix $\boldsymbol{E_2}$ and initial imperfection effect. Similar responses are observed in Figs. 11-12. These plates have simply supported boundary conditions on loaded ends and clamped conditions on unloaded edges. So, the mathematical model is expressed as Eq. (27).

Although, the imperfections have the same values but as it can be seen in these figures, the responses of dimensionless displacements and longitudinal load are completely different. As mentioned before, this difference is due to the effects of the bending-extensional coupling stiffness matrix. FG plate with positive imperfection initially deflects along the positive direction and gradually its deformation becomes negative.

4.3 FGM plates with un-symmetric imperfection

Imperfect square FGM plates with $2a/h = 20$ and with un-symmetric initial imperfection are investigated in this section. Material properties are similar to previous sections. All edges of the plates are simply-supported for out-of-plane deflection and in-plane boundary conditions are selected to be similar to previous sections. So, both essential and natural boundary conditions can be mathematically defined as Eq. (25).

The non-dimensional initial imperfection for these plates is expressed by the following relationship (Ghannadpour *et al.* 2017).

$$\bar{w} = \bar{w}_c \cos\left(\frac{\pi x}{2a}\right)\left(0.8433\left(\frac{2y}{b}\right)^3 - 0.84\left(\frac{2y}{b}\right)^2 - 0.837\left(\frac{2y}{b}\right) + 0.8457\right) \tag{29}$$

where $\bar{w}_c$ is introduced as an imperfection coefficient at the middle of the plate. It should be noted that the imperfection introduced in Eq. (29) has un-symmetrical shape whose maximum value occurs at $1/3$ of the plate's width. The nonlinear behaviors of the FG plates with un-symmetric initial imperfections correspond to $\bar{w}_c = 0.2h$ and $\bar{w}_c = 0.5h$ are represented for different volume fractions in Figs. 13-14, respectively. The results of this section, are also compared with finite element method as before. As it is observed, there is an excellent agreement between both methods.

In another investigation, FG plates with different shape of un-symmetrical initial imperfection are considered which is expressed by the following relationship (Ghannadpour and Barekati 2016)

$$\bar{w} = \bar{w}_c \cos\left(\frac{\pi x}{2a}\right)\left(1.7764\left(\frac{2y}{b}\right)^3 - 0.44525\left(\frac{2y}{b}\right)^2 - 1.78\left(\frac{2y}{b}\right) + 0.4420\right) \tag{30}$$

where $\bar{w}_c$ is initial deflection coefficient at the center of the plate. In this imperfection shape, the maximum initial imperfection occurs at $1/4$ of the plate's width. The post-buckling and nonlinear responses of the plates with coefficient of $\bar{w}_c = \pm 0.2h$and $\pm 0.5h$ and with different volume fraction indexes of n have been studied and illustrated in Figs. 15-16. All edges of the plates are simply-supported for out-of-plane deflection and loaded and unloaded edges are allowed to expand laterally. So, the mathematical model is expressed as Eq. (25).

It is observed that the shape and magnitude of initial imperfection affect the nonlinear behavior of plates. Also, it is seen in Fig. 16 that the curve corresponds to FG plate

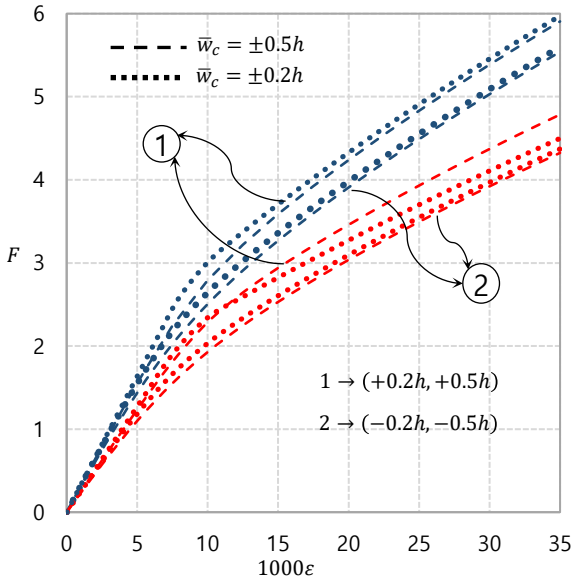

Fig. 15 Variation of longitudinal force versus end-shortening for FGPs with un-symmetric imperfection $\bar{w}_c = \pm 0.2h, \pm 0.5h$

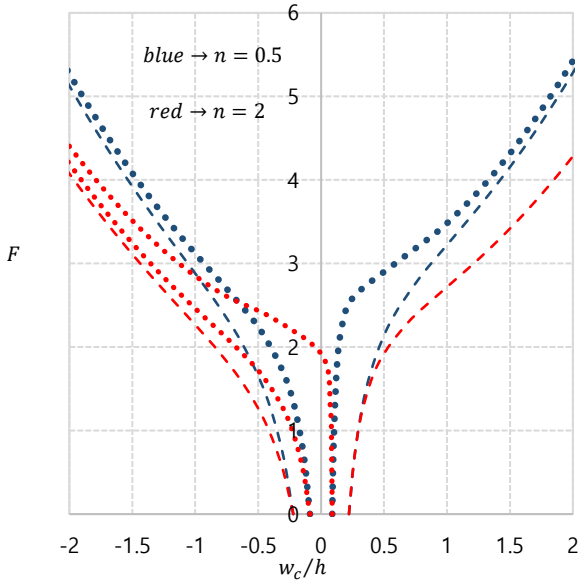

Fig. 16 Longitudinal force-central deflection for FGPs with un-symmetric imperfection $\bar{w}_c = \pm 0.2h, \pm 0.5h$

with $n = 2$and with positive initial imperfection of $+0.2h$ initially deflects along the positive direction and gradually its deformation becomes negative due to the effects of the bending-extensional coupling stiffness matrix. Such behavior is not seen in the FG plate with $n = 0.5$ due to the weaker effects of bending-extensional coupling coefficients.

It could also be expressed that the increase in the level of strain changes the shape of the deflection from un-symmetric to symmetric. Fig. 17 shows this behavior for plate with $\bar{w}_c = 0.2h$ and volume fraction index $n = 1$.

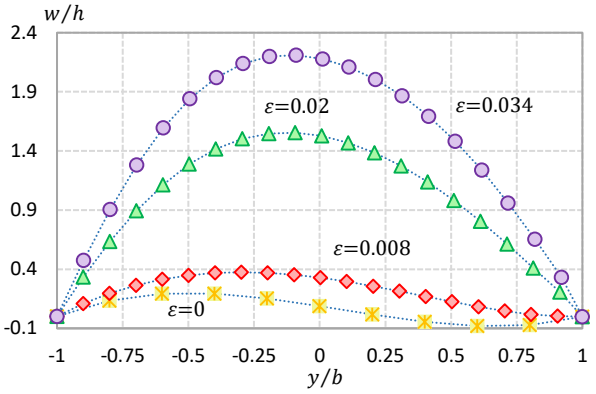

Fig. 17 Deflection shape across the plate with $\bar{w}_c = 0.2h$ for different values of end-shortening strain

5. Conclusions

A spectral collocation approach based on Legendre Basis Function (LBF) were investigated for the geometrically nonlinear and post-buckling analysis of FGM plates with and without geometric imperfection. This high accuracy mesh-less analysis was also conducted for nonlinear analysis of moderately thick FGM plates. So, this paper has extended a method for examination of the effects of initial symmetric and un-symmetric imperfection on post-buckling and nonlinear behaviors for moderately thick FGM plates with Legendre polynomials. Different boundary conditions and imperfection shapes including symmetric and un-symmetric shapes have been considered. It was shown how the shape and values of imperfection affect the post-buckling and nonlinear behaviors and also out of plane deflection shape of the plate. It was seen that when the plates have un-symmetrical initial shape, the increase in the level of loading changes the shape of the deflection from un-symmetric to symmetric. It is also important to note that, the methodology carried out here is completely unique in analyzing the nonlinear and post-buckling behaviors of FG plates, and due to a significantly lower number of terms used in the displacement fields, the solution is obtained much faster and more reliable than other taken methods in the literature. Using proposed method one can change basis, increase nodal densities and deal with complex geometries with sharp discontinues or growing crack. The presented technique gives better approximation and prevents any artificial discontinuity in the field and does not require the generation of meshes. It is very simple to implement due to no integration is required. The excellent accuracy in function fitting and simple imposition of essential and natural boundary conditions are other features of the present method.

References

Bakora, A. and Tounsi, A. (2015), "Thermo-mechanical post-buckling behavior of thick functionally graded plates resting on elastic foundations", *Struct. Eng. Mech.*, **56**(1), 85-106.

Banić, D., Bacciocchi, M., Tornabene, F. and Ferreira, A.J. (2017),

"Influence of Winkler-Pasternak foundation on the vibrational behavior of plates and shells reinforced by agglomerated carbon nanotubes", *Appl. Sci.*, **7**(12), 1-55.

Belinha, J. and Dinis, L.M.J.S. (2007), "Nonlinear analysis of plates and laminates using the element free Galerkin method", *Compos. Struct.*, **78**(3), 337-350.

Dai, K.Y., Liu, G.R., Lim, K.M., Han, X. and Du, S.Y. (2004), "A mesh-free radial point interpolation method for analysis of functionally graded material (FGM) plates", *Comput. Mech.*, **34**(3), 213-223.

Fantuzzi, N., Tornabene, F., Bacciocchi, M. and Dimitri, R. (2017), "Free vibration analysis of arbitrarily shaped functionally graded carbon nanotube-reinforced plates", *Compos. Part B.-Eng.*, **115**, 384-408.

Ferreira, A.J.M. (2013), "Bending and vibration of laminated plates by a layerwise formulation and collocation with radial basis functions", *Mech. Adv. Mater. Struct.*, **20**(8), 624-637.

Ghannadpour, S.A.M. and Alinia, M.M. (2006), "Large deflection behavior of functionally graded plates under pressure loads", *Compos. Struct.*, **75**(1), 67-71.

Ghannadpour, S.A.M. and Alinia, M.M. (2009), "Nonlinear analysis of pressure loaded FGM plates", *Compos. Struct.*, **88**(3), 354-359.

Ghannadpour, S.A.M. and Barekati, M. (2016), "Initial imperfection effects on post-buckling response of laminated plates under end-shortening strain using Chebyshev techniques", *Thin. Wall. Struct.*, **106**, 484-494.

Ghannadpour, S.A.M. and Ovesy, H.R. (2008), "An exact finite strip for the calculation of relative post-buckling stiffness of I-section struts", *Int. J. Mech. Sci.*, **50**(9), 1354-1364.

Ghannadpour, S.A.M., Kiani, P. and Reddy, J.N. (2017), "Pseudo spectral method in nonlinear analysis of relatively thick imperfect laminated plates under end-shortening strain", *Compos. Struct.*, **182**, 694-710.

Ghannadpour, S.A.M., Ovesy, H.R. and Nassirnia, M. (2012), "Buckling ana lysis of functionally graded plates under thermal loadings using the finite strip method", *Comput. Struct.*, **108**, 93-99.

Gilhooley, D.F., Batra, R.C., Xiao, J.R., McCarthy, M.A. and Gillespie, J.r. (2007), "Analysis of thick functionally graded plates by using higher-order shear and normal deformable plate theory and MLPG method with radial basis functions", *Compos. Struct.*, **80**(4), 539-552.

Huang, B.Z. and Atluri, S.N. (1995), "A simple method to follow post-buckling paths in finite element analysis", *Comput. Struct.*, **57**(3), 477-489.

Kar, V.R. and Panda, S.K. (2016), "Post-buckling behavior of shear deformable functionally graded curved shell panel under edge compression", *Int. J. Mech. Sci.*, **115**, 318-324.

Kar, V.R. and Panda, S.K. (2017), "Post-buckling analysis of shear deformable FG shallow spherical shell panel under non-uniform thermal environment", *J. Therm. Stress.*, **40**(1), 25-39.

Kar, V.R., Mahapatra, T.R. and Panda, S.K. (2017), "Effect of different temperature load on thermal post-buckling behavior of functionally graded shallow curved shell panels", *Compos. Struct.*, **160**, 1236-1247.

Kar, V.R., Panda, S.K. and Mahapatra, T.R. (2016), "Thermal buckling behavior of shear deformable functionally graded single/doubly curved shell panel with TD and TID properties", *Adv. Mater. Res.*, **5**(4), 205-221.

Katariya, P.V. and Panda, S.K. (2016), "Thermal buckling and vibration analysis of laminated composite curved shell panel", *Aircr. Eng. Aerosp. Tec.*, **88**(1), 97-107.

Katariya, P.V., Panda, S.K., Hirwani, C.K., Mehar, K. and Thakare, O. (2017), "Enhancement of thermal buckling strength of laminated sandwich composite panel structure embedded with shape memory alloy fiber", *Smart. Struct. Syst.*, **20**(5), 595-605.

Kim, Y.H. and Noor, A.K. (1996), "Buckling and post-buckling of composite panels with cutouts subjected to combined loads", *Fin. Elem. Anal. Des.*, **22**(2), 163-185.

Lee, Y.Y., Xin, Z. and Reddy, J.N. (2010), "Post-buckling analysis of functionally graded plates subject to compressive and thermal loads", *Comput. Meth. Appl. Mech. Eng.*, **199**(25), 1645-1653.

Lee, Y.Y., Zhao, X. and Liew, K.M. (2009), "Thermoelastic analysis of functionally graded plates using the element free kp-ritz method", *Smart Mater. Struct.*, **18**(3), 035007.

Liew, K.M. and Chen, X.L. (2004), "Mesh-free radial point interpolation method for the buckling analysis of mindlin plates subjected to in-plane point loads", *Int. J. Numer. Meth. Eng.*, **60**(11), 1861-1877.

Liu, G.R. and Chen, X.L. (2001), "A mesh-free method for static and free vibration analysis of thin plates of complicated shape", *J. Sound Vibr.*, **241**(5), 839-855.

Liu, G.R. and Gu, Y.T. (2001), "A point interpolation method for two-dimensional solids", *Int. J. Numer. Meth. Eng.*, **50**(4), 937-951.

Liu, L., Chua, L.P. and Ghista, D.N. (2007), "Mesh-free radial basis function method for static, free vibration and buckling analysis of shear deformable composite laminates", *Compos. Struct.*, **78**(1), 58-69.

Ovesy, H.R. and Ghannadpour, S.A.M. (2007), "Large deflection finite strip analysis of functionally graded plates under pressure loads", *Int. J. Struct. Stab. Dyn.*, **7**(2), 193-211.

Ovesy, H.R. and Ghannadpour, S.A.M. (2009), "An exact finite strip for the calculation of relative post-buckling stiffness of isotropic plates", *Struct. Eng. Mech.*, **31**(2), 181-210.

Ovesy, H.R., Ghannadpour, S.A.M. and Morada, G. (2005), "Geometric non-linear analysis of composite laminated plates with initial imperfection under end shortening, using two versions of finite strip method", *Compos. Struct.*, **71**(3), 307-314.

Ovesy, H.R., Ghannadpour, S.A.M. and Nassirnia, M. (2015), "Post-buckling analysis of rectangular plates comprising functionally graded strips in thermal environments", *Comput. Struct.*, **147**, 209-215.

Ovesy, H.R., Loughlan, J. and Ghannadpour, S.A.M. (2006), "Geometric non-linear analysis of channel sections under end shortening, using different versions of the finite strip method", *Comput. Struct.*, **84**(13), 855-872.

Panda, S.K. and Katariya, P.V. (2015), "Stability and free vibration behavior of laminated composite panels under thermo-mechanical loading", *Int. J. Appl. Comput. Math.*, **1**(3), 475-490.

Panda, S.K. and Singh, B.N. (2009), "Thermal post-buckling behavior of laminated composite cylindrical/hyperboloid shallow shell panel using nonlinear finite element method", *Compos. Struct.*, **91**(3), 366-374.

Panda, S.K. and Singh, B.N. (2010a), "Nonlinear free vibration analysis of thermally post-buckled composite spherical shell panel", *Int. J. Mech. Mater. Des.*, **6**(2), 175-188.

Panda, S.K. and Singh, B.N. (2010b), "Thermal post-buckling analysis of a laminated composite spherical shell panel embedded with shape memory alloy fibers using non-linear finite element method", *Proc. Inst. Mech. Eng. C: J. Mech. Eng. Sci.*, **224**(4), 757-769.

Panda, S.K. and Singh, B.N. (2011), "Large amplitude free vibration analysis of thermally post-buckled composite doubly curved panel using nonlinear FEM", *Fin. Elem. Anal. Des.*, **47**(4), 378-386.

Panda, S.K. and Singh, B.N. (2013a), "Nonlinear finite element analysis of thermal post-buckling vibration of laminated composite shell panel embedded with SMA fiber", *Aerosp. Sci. Technol.*, **29**(1), 47-57.

Panda, S.K. and Singh, B.N. (2013b), "Post-buckling analysis of laminated composite doubly curved panel embedded with SMA fibers subjected to thermal environment", *Mech. Adv. Mater. Struct.*, **20**(10), 842-853.

Panda, S.K. and Singh, B.N. (2013c), "Large amplitude free vibration analysis of thermally post-buckled composite doubly curved panel embedded with SMA fibers", *Nonlin. Dyn.*, **74**(1-2), 395-418.

Qian, L.F. and Batra, R.C. (2004), "Transient thermoelastic deformations of a thick functionally graded plate", *J. Therm. Stress.*, **27**(8), 705-740.

Reddy, J.N. (2004), *Mechanics of Laminated Composite Plates and Shells, Theory and Analysis*, CRC Press, Boca Raton, U.S.A.

Sherafat, M.H., Ghannadpour, S.A.M. and Ovesy H.R. (2013), "Pressure loading, end-shortening and through-thickness shearing effects on geometrically nonlinear response of composite laminated plates using higher order finite strip method", *Struct. Eng. Mech.*, **45**(5), 677-691.

Sherafat, M.H., Ovesy, H.R. and Ghannadpour, S.A.M. (2013), "Buckling analysis of functionally graded plates under mechanical loading using higher order functionally graded strip", *Int. J. Struct. Stab. Dyn.*, **13**(6), 1350033.

Singh, S.B. and Kumar, D. (2008), "Post-buckling response and failure of symmetric laminated plates with rectangular cutouts under uniaxial compression", *Struct. Eng. Mech.*, **29**(4), 455-467.

Singh, S.B. and Kumar, D. (2010), "Post-buckling response and failure of symmetric laminated plates with rectangular cutouts under in-plane shear", *Struct. Eng. Mech.*, **34**(2), 175-188.

Sofiyev, A.H. (2007), "Vibration and stability of composite cylindrical shells containing a FG layer subjected to various loads", *Struct. Eng. Mech.*, **27**(3), 365-391.

Tornabene, F. and Viola, E. (2009), "Free vibration analysis of functionally graded panels and shells of revolution", *Meccan.*, **44**(3), 255-281.

Tornabene, F. (2009), "Free vibration analysis of functionally graded conical, cylindrical shell and annular plate structures with a four-parameter power-law distribution", *Comput. Meth. Appl. Mech. Eng.*, **198**(37-40), 2911-2935.

Tornabene, F., Fantuzzi, N. and Bacciocchi, M. (2017), "Linear static response of nanocomposite plates and shells reinforced by agglomerated carbon nanotubes", *Compos. Part B-Eng.*, **115**, 449-476.

Tornabene, F., Fantuzzi, N., Bacciocchi, M., Viola, E. and Reddy, J.N. (2017), "A numerical investigation on the natural frequencies of FGM sandwich shells with variable thickness by the local generalized differential quadrature method", *Appl. Sci.*, **7**(2), 1-39.

Wang, J.G. and Liu, G.R. (2002), "A point interpolation mesh-less method based on radial basis functions", *Int. J. Numer. Meth. Eng.*, **54**(11), 1623-1648.

Zhao, X., Lee, Y.Y. and Liew, K.M. (2009), "Mechanical and thermal buckling analysis of functionally graded plates", *Compos. Struct.*, **90**(2), 161-171.